CNTs in Optoelectronic Devices: New Structural and Photophysical Insights on Porphyrin-DWCNTs Hybrid Materials

Claudia Aurisicchio, Riccardo Marega, Valentina Corvaglia, John Mohanraj, Romain Delamare, Dana Alina Vlad, Cristian Kusko, Constantin Augustin Dutu, Andrea Minoia, Gaëlle Deshayes, Olivier Coulembier, Sorin Melinte, Philippe Dubois,* Roberto Lazzaroni,* Nicola Armaroli,* and Davide Bonifazi**

The preparation and physical characterization of diverse porphyrin-derived double-walled carbon nanotubes (DWCNTs) conjugates are described. A porphyrin molecule is covalently linked and physically adsorbed to COOH-derived DWCNTs. The photophysical properties of all porphyrin-CNTs derivatives are studied in solution and in polymeric matrices. Definitive experimental evidence for photoinduced electron and/or energy transfer processes involving the porphyrin chromophores and the CNT wall is not obtained, but solid-state UV-vis absorption profiles display electronic transitions fingerprinting *J*- and *H*- type aggregates, where porphyrin molecules intermolecularly interact "head-to-tail" and "face-to-face", respectively. In parallel, molecular modeling based on force-field simulations is performed to understand the structure of the porphyrin-CNTs interface and the nature of the interactions between the porphyrins and the DWCNTs. Finally, multilayered-type devices are fabricated with the aim of investigating the interaction of the porphyrin-derived DWCNTs with poly(3-hexylthiophene)-pyrene matrices containing small amounts of 1-[3-(methoxycarbonyl)propyl]-1-phenyl-[6.6]C_{61}.

1. Introduction

In a time when the need to preserve natural resources for future generations is gaining public awareness, the exploitation of sunshine as a clean, abundant, and inexhaustible source of energy is one of the key strategies to stimulate an innovative and more sustainable global economy.[1] In this context, photovoltaic (PV) devices have attracted the highest attention as alternative electricity generators.[2] Nowadays, solar PV devices belong to three main classes: inorganic (e.g., silicon photoelectric cells), organic (e.g., bulk-heterojunction PV cells), and photoelectrochemical cells (e.g., dye sensitized solar cells). Among those, organic photovoltaic (OPV) systems[3] are prepared by cheap solution-based methods and offer high mechanical flexibility for preparing low-cost versatile and large photovoltaic

C. Aurisicchio, Dr. R. Marega, Prof. D. Bonifazi
Department of Chemistry and Namur Advanced Research College (NARC)
University of Namur
Rue de Bruxelles 61, Namur B-5000, Belgium
E-mail: davide.bonifazi@fundp.ac.be

V. Corvaglia, Dr. D. Bonifazi
Department of Pharmaceutical and Chemical Sciences
University of Trieste
Piazzale Europa 1, 34127 Trieste, Italy

J. Mohanraj, Dr. N. Armaroli
Molecular Photoscience Group
Istituto per la Sintesi Organica e la Fotoreattività del CNR
Via P. Gobetti 101, 40129 Bologna, Italy
E-mail: nicola.armaroli@cnr.it

Dr. R. Delamare, Dr. D.-A. Vlad, C. A. Dutu, Dr. S. Melinte
Université catholique de Louvain
ICTM Institute
Louvain La Neuve B-1348, Belgium
E-mail: sorin.melinte@uclouvain.be

Dr. C. Kusko
IMT-Bucharest Institute
Str. Erou Iancu Nicolae 126A,
077190 Bucharest, Romania

Dr. A. Minoia, Prof. R. Lazzaroni
Laboratory for Chemistry of Novel Materials
Center of Innovation and Research in Materials & Polymers (CIRMAP)
University of Mons-UMONS/Materia Nova
20 Place du Parc, Mons B-7000, Belgium
E-mail: roberto.lazzaroni@umons.ac.be

Dr. G. Deshayes, Dr. O. Coulembier, Prof. P. Dubois
Laboratory of Polymeric and Composite Materials
Center of Innovation and Research in Materials & Polymers (CIRMAP)
University of Mons-UMONS
Place du Parc 20, Mons B-7000, Belgium
E-mail: philippe.dubois@umons.ac.be

DOI: 10.1002/adfm.201102632

surfaces. In these devices, photoinduced charge separation processes occur at the interface between two distinct materials, namely an electron-donor (D) and an electron-acceptor (A). The interface between these two materials constitutes the analogue of the inorganic semiconductor p–n junctions. State-of-the-art organic solar cells are made with disordered bulk heterojunctions, in which electron-donor and -acceptor molecules are intimately mixed to form an interpenetrating phase network at the nanoscale level.[4] The performance of such solar cells dramatically depends on the nanomorphology of the donor-acceptor hybrids and on the layer conductivity. At present, bulk heterojunction OPV cells have still a limited stability and a low efficiency (around 8% at their best)[5] if compared to their inorganic analogues. The low efficiency is mainly due to the fact that the average distance over which an exciton can diffuse between its generation and its recombination is rather short, so that only excitons produced close enough to the heterojunction are effective for electricity generation.[3] In order to enhance OPV performance, conjugated polymer-fullerene thin films have been prepared because of their high charge mobility, crystallinity, and thermal stability.[6] Similarly, carbon nanotubes (CNTs) have emerged as active materials to be incorporated in organic photovoltaics[7] due to their high charge mobility as well as chemical inertness.[8] However, key-issues still need to be addressed for the realization of multifunctional CNTs-based nanoconjugates and/or nanohybrid PV systems; peculiarly difficult is the reliable and reproducible control of the surface chemistry of CNTs and of their organization within the active layer owing to their particular intermolecular cohesive forces (0.5 eV nm^{-1}).[9] In fact, CNTs tend to strongly aggregate both in solution and in the solid state, forming bundled structures that often cause a low reproducibility of the conducting properties and display a percolation threshold of a few percent.[9]

The chemical derivatization, either covalent[10–13] or non-covalent,[14–17] turned out to be an efficient strategy to create easy-to-process CNT-based materials.[18] In particular, the incorporation of photoactive antenna chromophores (displaying high extinction coefficient in the visible region of the solar spectrum) such as porphyrins[19] is one of the most popular routes to engineer charge-separation and photovoltaic conversion.[20] Depending on the organization of the architecture, photophysical investigations have shown that supramolecularly-assembled porphyrin-CNTs conjugates can undergo photoinduced electron or energy transfer phenomena, suggesting strong electronic communications between the chromophoric moieties and the CNTs' framework.[15–17] On the contrary, conjugates consisting of covalently grafted porphyrin-CNT materials showed a different behavior. Specifically, photoinduced electron and energy transfer processes have been detected in systems where strong donor-acceptor interactions could be established,[10,12] whereas they were absent when the structure and the flexibility of the covalent linkage between the porphyrin unit and the CNTs did not allow strong electronic contacts.[13]

To gain insight into the structural and electronic properties of CNT-porphyrin conjugates, we report the preparation and physical characterization of some porphyrin-derived double-walled carbon nanotube (DWCNTs) conjugates (**Scheme 1**). With respect to single-wall counterparts, DWCNTs can be selectively functionalized at the external sidewall without disrupting the internal carbon layer thus keeping unaltered the CNT conductive properties. Therefore, oxidized DWCNTs (***ox*-DWCNTs**) have been covalently functionalized or physically absorbed to porphyrin molecules producing the three derivatives, **1-DWCNTs**, **1@(1-DWCNTs)** and **1@DWCNTs**. The structural properties of all porphyrin-DWCNTs conjugates have been fully investigated via thermogravimetric analysis (TGA), energy dispersive X-ray spectroscopy (EDX), X-ray photoelectron spectroscopy (XPS), transmission electron microscopy (TEM), atomic force microscopy (AFM), and dynamic light scattering (DLS) experiments. Molecular modeling based on force-field simulations was employed to understand the nature of the interactions between the two species and to determine their most stable conformation. The photophysical properties of the porphyrin-CNTs derivatives have been studied through absorption and emission spectroscopies both in solution and solid state. Finally, in order to evaluate both morphological and conducting properties of the porphyrin-DWCNTs derivatives as dopants in active layers of photovoltaic cells, we have fabricated multilayered-type devices with the aim of investigating the interaction of the porphyrin-derived DWCNTs with a poly(3-hexylthiophene) end-capped by a pyrene unit (P3HT-Py) and containing small amounts of 1-[3-(methoxycarbonyl)propyl]-1-phenyl-[6.6]C_{61} ([60]PCBM). In particular, current density–voltage (*J*–*V*) and external quantum efficiency (EQE) measurements have been performed to evaluate the electronic properties of the organic active layer.

2. Results and Discussion

2.1. Synthesis

The synthesis of the starting materials and the final porphyrin-DWCNTs conjugates is outlined in Scheme 1. The chosen porphyrin derivative, molecule **1**, is based on a tetrapyrrolic core differently substituted at the four *meso*-positions by three solubilizing 4-*tert*-butyl substituents and one benzyl hydroxyl function suitable for the subsequent ester linkage. Due to the straightforward protocol, the mixed condensation reaction was selected as a procedure for the preparation of the porphyrin derivatives.[21] Therefore, methyl ester porphyrin derivative **2** has been prepared following the typical Lindsay's procedure[22] using a 4:3:1 mixture of pyrrole, 4-*tert*-butylbenzaldheyde, and methyl 4-formyl-benzoate in the presence of $BF_3 \cdot OEt_2$. Consecutive oxidation with 2,3-dichloro-5,6-dicyano-1,4-benzoquinone (DDQ) (Scheme 1, path a) led to molecule **2** in good yield. Monosubstituted porphyrin **1** was then prepared in 70% yield from precursor **2** with $LiAlH_4$ (Scheme 1, path b). In parallel, ***ox*-DWCNTs** were prepared following three oxidative steps (Scheme 1, path ***c***). Pristine DWCNTs, ***p*-DWCNTs**, were first treated with an aq. solution of H_2O_2 (15%), following a recently reported mild procedure,[23,24] to open CNTs tips and shorten their length by oxidative attacks. Subsequently, heat treatment at 450 °C for 45 min under an external air purge was carried out to remove the amorphous carbonaceous materials, decreasing the carbon-coating of the metallic impurities and maximize the tip destruction. A final 1 h treatment with a 3:1 ratio mixture

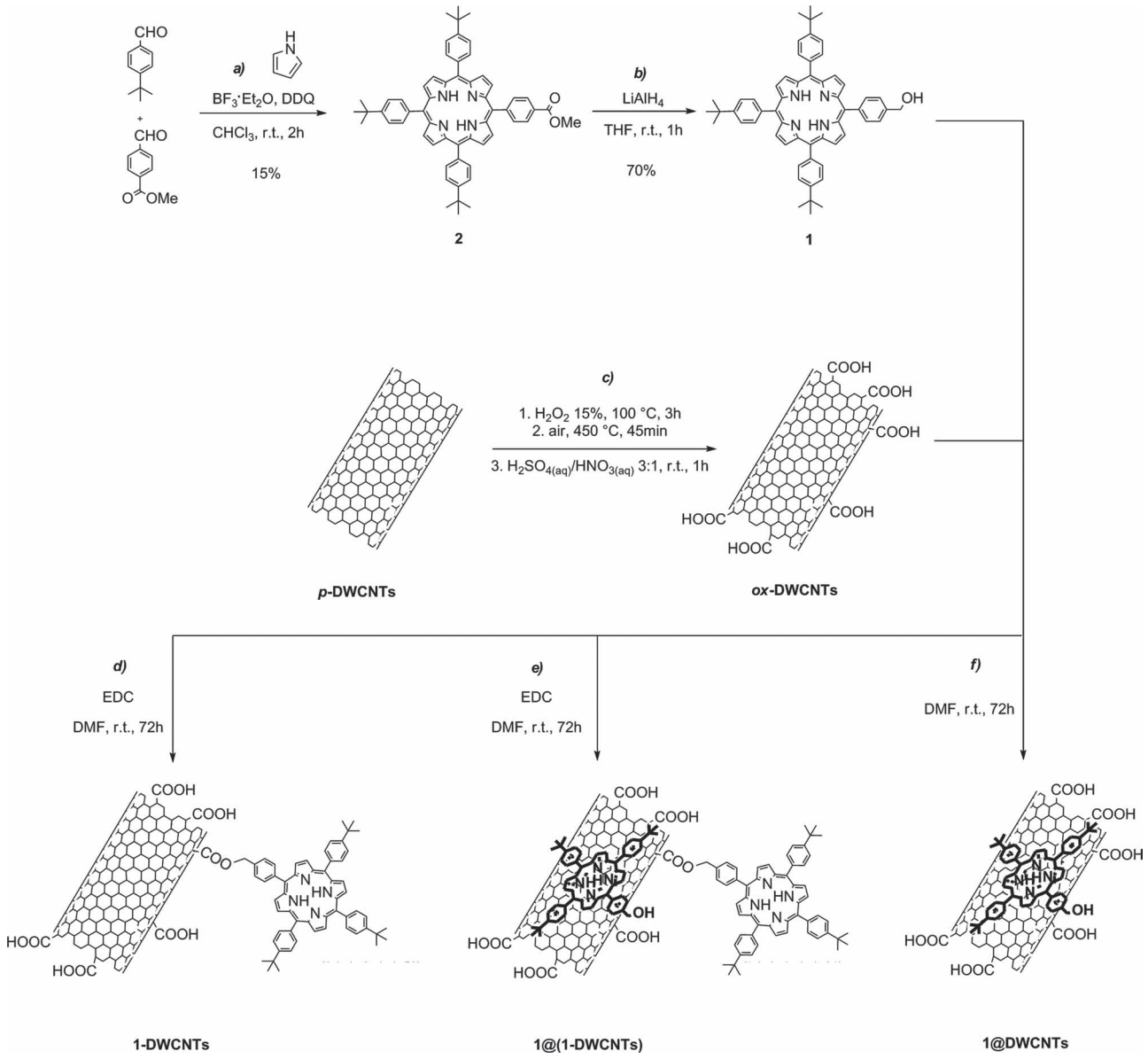

Scheme 1. Synthetic pathways toward the preparation of porphyrin-decorated DWCNTs. EDC: *N*-[3-(dimethylamino)propyl]-*N'*-ethylcarbodiimide; HOBt: *N*-hydroxybenzotriazole; NHS: *N*-hydroxysuccinimide.

of aq. H_2SO_4 (95%) and HNO_3 (65%) solutions led to the final ***ox*-DWCNTs**. This step was performed to increase the number of carboxylic acid functionalities and to further remove metallic residues deriving from the catalyst.

2.2. Structural and Morphological Characterizations of the Porphyrin-DWCNTs Derivatives

As a first method to characterize the structural changes induced by the oxidative steps, X-ray-based techniques were utilized, aiming at a qualitative and quantitative assessment of the chemical composition of the ***ox*-DWCNTs**. The EDX analysis of 150 μm^2 spots of both ***p*-DWCNTs** and ***ox*-DWCNTs** is reported in Figure S1 (Supporting Information). The atomic percentage (at%) compositions for C (0.277 keV), O (0.525 keV), and Fe (6.398 keV) are 94.46, 4.99, and 0.54 for ***p*-DWCNTs** and 87.80, 12.08, and 0.11 for ***ox*-DWCNTs**, respectively. These data indicate that the oxidative treatments increased the O at% content for ***ox*-DWCNTs** (+7.09 at%), decreasing simultaneously the Fe at% to one fifth of the initial value (–0.43 at%), thus indicating an enhanced purity of the sample. These results are in good agreement with those obtained by XPS investigation (Figure S2, Supporting Information). Specifically, also this

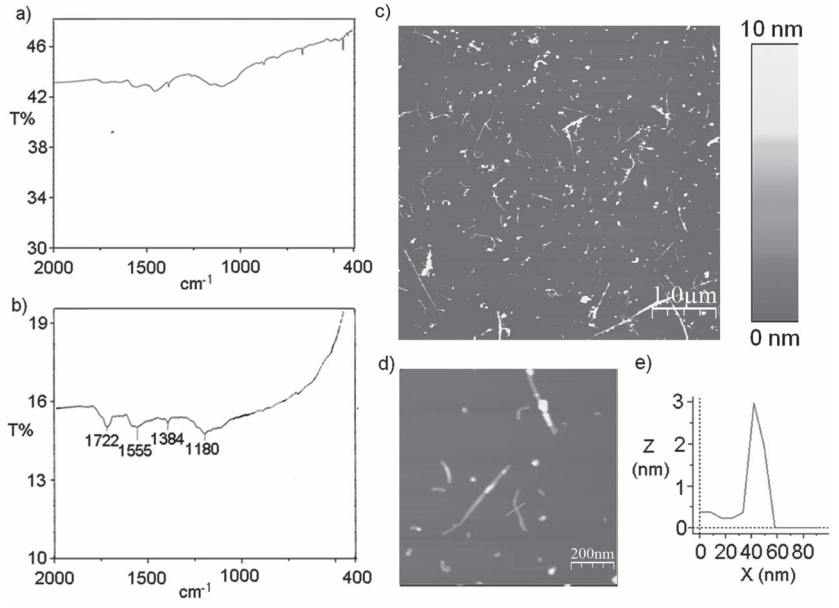

Figure 1. ***ox*-DWCNTs** characterization: a,b) excerpts of the IR spectra of ***p*-DWCNTs** and ***ox*-DWCNTs**, respectively. A clear increment of the typical –COOH-centered stretching signal is observed moving from the a) pristine to the b) oxidized sample, supporting the occurred introduction of oxygenated functionalities mainly as carboxylic acids groups. c) TM-AFM image (air, 298 K) of a portion of mica surface after the deposition of a ***ox*-DWCNTs** dispersion in dimethylformamide (DMF). Isolated and bundled short CNTs are present on the surface; d) higher magnification TM-AFM image and e) related height cross-section highlighting the presence of very short isolated DWCNTs.

technique assessed a clear increase of the O at% content in the oxidized samples (5.94 at% for O1s at 532.3 eV, meaning a +3.06 at% with respect to ***p*-DWCNTs**). These results are in good accordance with previous findings in the literature, for which mineral acid treatments of CNTs induced high increase of the O at% content, as a consequence of the enhancement of O-bearing groups mainly ascribed to the carboxylic acid functionalities.[25] In fact, by comparing the IR spectra of the samples before and after the oxidation (**Figure 1**a,b), a clear enhancement of the intensity of the CO-centered vibrational transition at 1722 cm^{-1} corresponding to COOH functionalities is clearly distinguishable, corroborating the carboxylic acid character of the oxidized species.

A further confirmation of the presence of -COOH functionalities was provided by the TGA investigation under inert atmosphere (N_2). The weight-loss plots relative to ***p*-DWCNTs** (Figure S3a, Supporting Information) and ***ox*-DWCNTs** (Figure S3b, Supporting Information) display two pyrolytic events: one occurs between 100 °C and 500 °C, where the defunctionalization of CNTs framework takes place, and a second between 650 °C and 850 °C, where CNTs undergo thermal decomposition. During the first event, the weight losses for ***p*-DWCNTs** and ***ox*-DWCNTs** are about 1% and 6% w/w, respectively. Assuming that the pyrolytic step is mainly caused by thermal decarboxylation reactions, a mass content of 1.4 μmol mg^{-1} of –COOH functionalities is estimated.

In a previous report, we have described that, using dilute solutions of H_2O_2, the shortening and opening of the end caps of DWCNTs could be efficiently achieved, as shown by AFM and high-resolution TEM investigations, respectively.[24] As in this work we have introduced an additional oxidative treatment with mineral acids (see above), a further microscopic analysis resulted to be necessary in order to evaluate the effectiveness of the employed oxidizing conditions on the shortening process. In this respect, after the third oxidative step, shortened isolated and bundled CNTs were observed by TEM imaging (Figure S4, Supporting Information). Nonetheless, low resolution TEM imaging techniques have a poor *Z*-resolution, which makes difficult the differentiation between isolated and bundled CNTs and therefore difficult the statistical evaluation of CNTs' length. Considering the nanoscopic resolution of the scanning probe microscopic (SPM) techniques, tapping-mode AFM (TM-AFM) imaging resulted an efficient technique to evaluate the tube length and diameter. Therefore, deposits of ***ox*-DWCNTs** were imaged on mica after spin-coating a small amount of ≈0.2 mg mL^{-1} DMF solution. A typical TM-AFM height image of such surfaces is reported in Figure 1c. By evaluating the cross-section height values for all the cylindrical objects present on different portions of the mica surface, it was possible to distinguish isolated and bundled CNTs as tubular structures with height values ranging from 3 nm (isolated tubes, Figure 1d,e) to more than 10 nm (bundles, Figure S5, Supporting Information). Using the WSxM 2.1 software (Nanotec Electronica, Spain), the tubes found on the surface were measured (n = 400) and their lengths statistically analyzed. An average of ***ox*-DWCNTs** length of 234 ± 167 nm was then estimated, a much lower value compared to the 534 ± 380 nm obtained in our former study.[24] The statistical analysis is more meaningful if associated with the frequency histograms depicted in Figure S6 (Supporting Information), where the frequencies of the observed lengths have been plotted as functions of the different dimensional classes. From these histograms, it is clearly visible that the most frequent CNTs lengths are comprised in the range between 100 and 250 nm (Figure S6a, Supporting Information), with 90% of the measured objects being shorter than 400 nm (Figure S6b, Supporting Information).

The as-prepared ***ox*-DWCNTs** were further used for the synthesis of the porphyrin-DWCNTs conjugates: **1-DWCNTs**, **1@(1-DWCNTs)** and **1@DWCNTs**. As depicted in Scheme 1, **1-DWCNTs** have been prepared upon sonication of a dispersion of ***ox*-DWCNTs** in DMF in the presence of **1** and EDC (Scheme 1, path d).[24,26] The final product was precipitated from DMF upon addition of H_2O to remove the excess of coupling agent and washed several times with $CHCl_3$ to completely discard the excess of non-reacted **1**. Meanwhile, following a slightly different protocol, conjugates **1@(1-DWCNTs)** were prepared (Scheme 1, path e). In this case, in order to preserve the adsorbed layer of **1** non-covalently attached to the tube walls, the adduct was precipitated from H_2O and then directly

Table 1. Compositional data obtained from XPS analysis of the investigated CNTs derivatives.

Sample	C at%	N at%	O at%
***p*-DWCNTs**	97.1	-	2.9
***ox*-DWCNTs**	94.0	-	6.0
1-DWCNTs	92.5	1.1	6.4
1@(1-DWCNTs)	89.4	1.8	8.8
1@DWCNTs	92.3	0.4	7.3

isolated through precipitation from acetone. Finally, non-covalent derivatives **1@DWCNTs** were synthesized following the same experimental conditions as those used to prepare **1-DWCNTs** but without EDC (Scheme 1, path f).

In order to investigate the degree of functionalization, XPS and TGA measurements were carried out. The XPS data are presented in **Table 1** (Figure S7, Supporting Information). As expected, all samples present the signatures of C and O atoms, but only those bearing the porphyrin fragments exhibit the presence of the N signature (N 1s at 400.0 eV). Notably, going from the non-covalent **1@DWCNTs** (0.4 at%) to the covalent **1-DWCNTs** conjugate (1.1 at%), up to complex **1@(1-DWCNTs)** (1.8 at%) a net increase of the N atomic percentage has been observed. The maximum loading of N atoms occurs in the covalent samples as well as in the case of complex **1@(1-DWCNTs)** due to the additional layer of physisorbed porphyrin molecules. Similarly, the results obtained from TGA (the temperature modulated and differential thermogravimetric plots are reported in **Figure 2** and Figure S8, Supporting Information) follow the same trend as that observed by the XPS analysis.

The pyrolysis of porphyrin **1** alone clearly appears with a prominent weight loss in the temperature range between 420 °C and 600 °C (Figure 2b). This weight loss step is also easily retrieved in the plot of **1@(1-DWCNTs)** complex proving the presence of porphyrin molecules (Figure 2c, band c). The differential plot of **1@(1-DWCNTs)** reports two other pyrolytic events between 100 °C and 400 °C (Figure 2c, bands a-b). These peaks can be interpretated as the signature of the pyrolysis of both EDC-functionalities and unreacted carboxylic groups attached on the CNTs frameworks. Once the pyrolysis of **1** has occurred, after 600 °C, **1@(1-DWCNTs)** was subjected to a 25.6% w/w loss, while **1-DWCNTs** and **1@DWCNTs** (Figure S8, Supporting Information) presented weight losses of 9.7% w/w and 8.5% w/w, respectively. Hence, TGA observations corroborate the XPS measurements attesting the higher loading of molecule **1** on the hybrid complex **1@(1-DWCNTs)**, also highlighting the efficiency of the purification steps carried out on the covalent derivative to remove the exceeding porphyrin quantities.

As a consequence of the presence of the covalently and non-covalently appended porphyrin units, the porphyrin-bearing DWCNTs show better dispersability than ***ox*-DWCNTs** in organic solvents such as DMF and $CHCl_3$. Interestingly, whereas conjugates **1-DWCNTs** and **1@DWCNTs** form stable dispersions, ***ox*-DWCNTs** show extensive precipitation after an initial apparent dissolution. This indirectly indicates that the

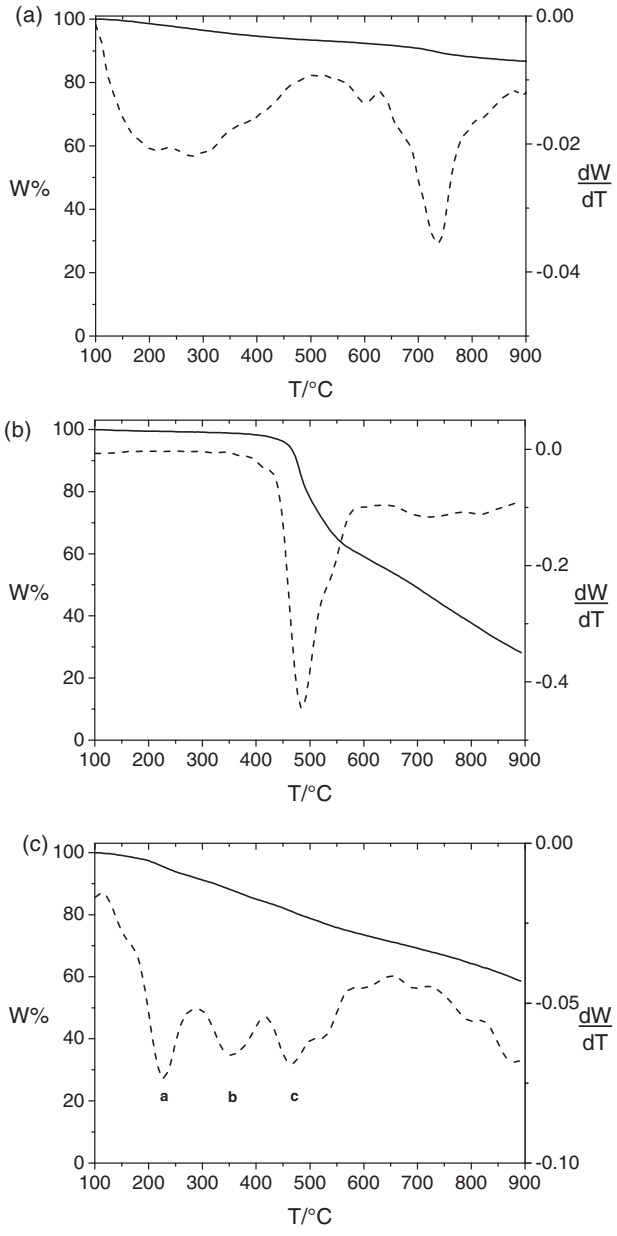

Figure 2. Temperature-modulated (——) and differential (——) gravimetric plots of a) ***ox*-DWCNTs**, b) **1**, and c) **1@(1-DWCNTs)**, recorded under N_2 atmosphere with a thermal increase of 10 °C min^{-1}. The TGA and DTGA plots for **1-DWCNTs** and **1@DWCNTs** are shown in Figure S8 (Supporting Information).

amount of CNTs dispersed in solution is expected to be substantially larger for **1-DWCNTs** and **1@DWCNTs** samples, thus enabling a more thorough characterization of the DWCNTs derivatives using optical spectroscopy. Although solutions of DWCNTs derivatives are transparent in DMF and $CHCl_3$ and do not exhibit any floating matter by visual inspection, the DWCNTs derivatives are, in fact, dispersed in a stable colloidal-like state. This has been confirmed by DLS measurements which displayed the presence of two groups of objects with

Table 2. Particle sizes distribution of the DWCNTs conjugates in DMF and $CHCl_3$ dispersions as evaluated from DLS.

Sample	Particle Size [nm]	
	DMF dispersion	$CHCl_3$ dispersion
***ox*-DWCNTs**	290[a], 60	[b]
1-DWCNTs	300, 90	730, 300
1@DWCNTs	400, 100	470[a], 160

[a]Due to very limited dispersibility of ***ox*-DWCNTs**, the measurements for such materials have been carried out after removing all the floating DWCNTs, so the concentration of dispersed tubes is lower compared to the other samples; [b]Impossible to be measured due to the large size of agglomerates.

different mean size (**Table 2**). In particular, the size distributions of the suspended carbon nanotube derivatives in clear, eye-transparent DMF and $CHCl_3$ dispersions of **1-DWCNTs**, **1@DWCNTs** and ***ox*-DWCNTs** are shown in **Figure 3**, **4** and Figure S9 (Supporting Information), respectively; the particle sizes are listed in Table 2.

From Table 2, it is clear that the particle sizes of the porphyrin-bearing DWCNTs hybrids in the dispersion are larger than that of the oxidized precursor, ***ox*-DWCNTs**. This is a consequence of the reduced bundling behavior of the functionalized DWCNTs caused by the presence of the porphyrin moieties, which impart better solubility to the hybrid material (i.e. increasing the number of large particles stable in solution). In the case of ***ox*-DWCNTs**, the larger nanotubes easily entangle and form large bundles that are more insoluble and quickly collected in the precipitate; accordingly, only very small and short CNTs remain in solution. However, all dispersions are not optimal for photophysical investigations because they undergo light scattering and prevent quantitative optical measurements (vide infra), particularly by means of transient spectroscopy upon intense laser excitation.

2.3. Modeling of the Conformational Properties of Porphyrin-DWCNTs Derivatives

Force field-based simulations using a combined molecular mechanics and molecular dynamics approach have been carried out in order to gain insight on the interactions between the porphyrin molecule and the nanotube framework. For simplicity, single-walled CNTs (SWCNTs) were considered, mimicking the outer shell of the DWCNTs.

As reported earlier for covalently-linked fullerene-porphyrin conjugates,[27] several conformational equilibria can occur in solution.[28,29] Likewise, a dynamic equilibrium between "loose" and "tight" porphyrin-CNTs pairs, in which the carbon nanotube and the porphyrin are in the "face-to-face" conformation in the ground state, can be considered (**Figure 5**). The "tight" and the "loose" conformation differ in the distance between the porphyrin and the CNTs and in their solvation.[30] The aim of the modeling here presented is thus to determine the most probable conformation of the porphyrin unit on the CNT wall and to quantify the strength of the interaction between the two species. Two situations were modeled with the porphyrin molecule either simply physisorbed on the CNT surface (i.e., **1@DWCNTs**)

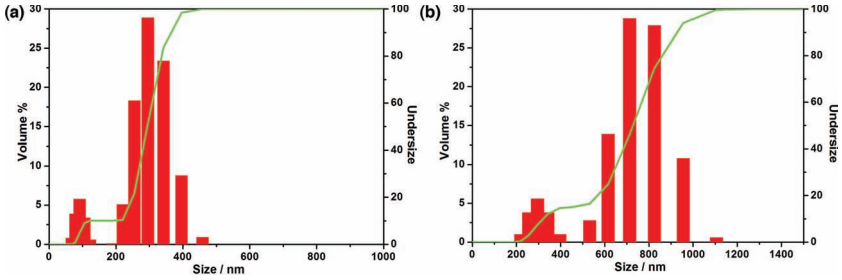

Figure 3. Size distribution of DWCNTs bundles in a) DMF and b) $CHCl_3$ dispersion of **1-DWCNTs**. For details see the Experimental Section.

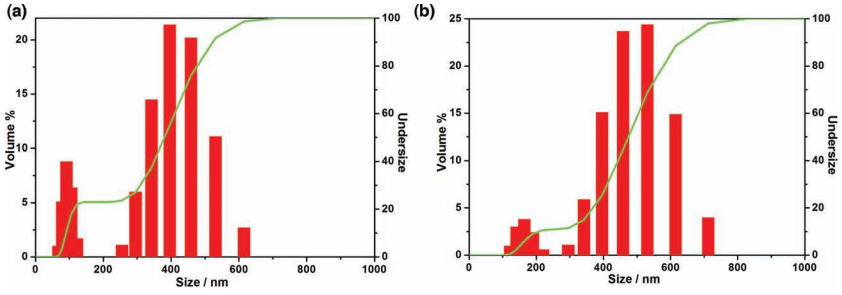

Figure 4. Size distribution of **1@DWCNTs** in a) DMF and b) $CHCl_3$. For details see the Experimental Section.

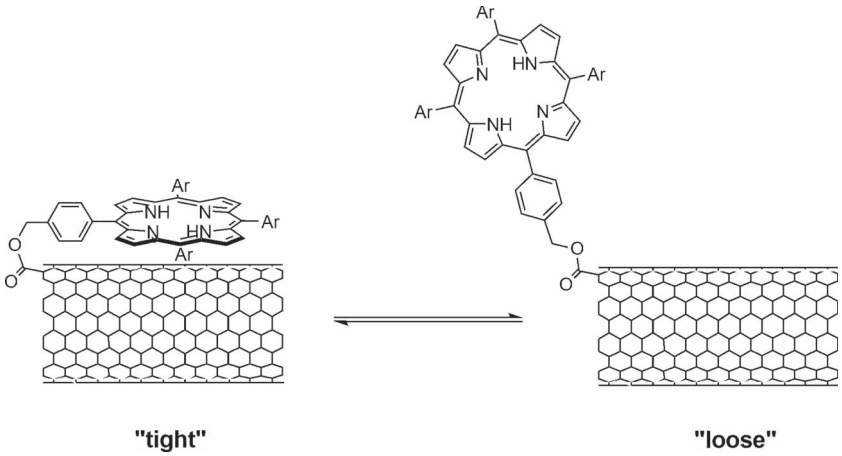

Figure 5. Schematic representations of the dynamic equilibrium existing between the "tight" and "loose" conformations of **1-DWCNTs**, when **1** is linked to the tips. The same equilibrium may exist also when the porphyrin fragment is linked to the walls of the DWCNTs. Ar stands for 4-(*tert*-butyl)phenyl.

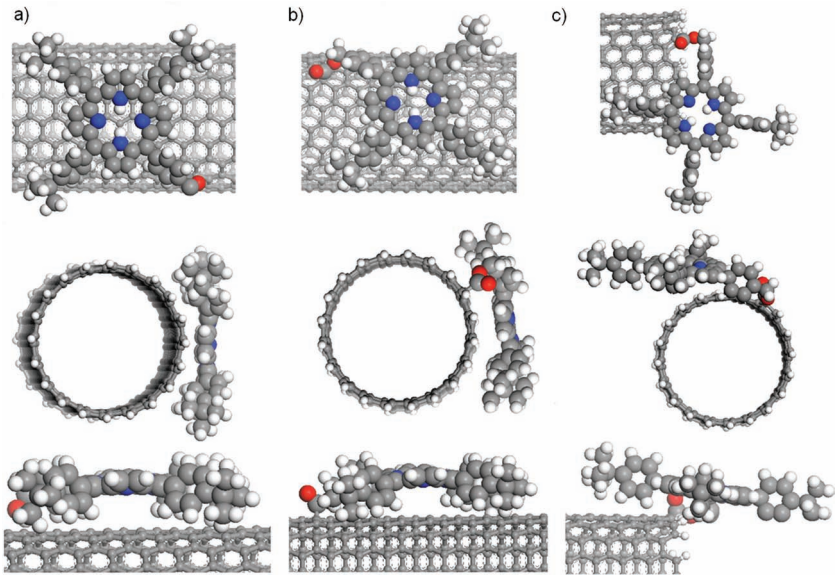

Figure 6. Top, front and side views for a) a porphyrin molecule physisorbed and covalently-bound to the nanotube b) wall or c) tips in a "tight" conformation.

or chemically grafted on the CNTs framework via a $COOCH_2$ linker (i.e., **1-DWCNTs**). For the covalent conjugate, two different grafting sites were considered: along the wall or at the edge of the open tips. **Figure 6** shows the top, front and side views for the three structural situations: in a) the porphyrin is physisorbed, while in (b) and (c) the porphyrin fragment is covalently bound to the wall and at tips, respectively. In structures (a) and (b), the tetrapyrrolic ring is roughly parallel to the nanotube surface: its core is slightly bent, with a mean distance of 0.35 nm from the nanotube. This value is typical of π-stacking and the slight bending of the core allows for optimal π–π interactions. In (c), the porphyrin core is not directly interacting with the nanotube and the molecule remains flat. Note that in all three cases, CH-π interactions are present between the side groups and the nanotube surface.

The potential energy for the physisorbed system cannot be strictly compared with the covalent systems, because of the different atomic compositions. Nevertheless some useful information can be obtained. The adsorption energy for a single physisorbed porphyrin molecule interacting with the CNT wall is about –60 kcal mol^{-1}. Consistently, the comparison for the two grafted arrangements shows that system (b) is about 60 kcal mol^{-1} more stable than system (c), reflecting larger van der Waals interactions between the porphyrin and the nanotube external wall when the molecule is grafted along the side. Notably, the flexibility of the linker can allow for conformations in which the end-grafted porphyrin is partly adsorbed on the CNT wall (vide supra).

Since the formation of carboxylic acids is expected to prominently take place at the tube ends, it is also relevant to model the presence of more than one porphyrin molecule covalently attached at the CNT edge. We have thus investigated systems having two porphyrin fragments covalently bound at the nanotube tip: the first porphyrin is attached to a fixed position and the second one is attached at an increasing distance from the first one. The various possibilities are denoted as 1–2, i.e., the two molecules are attached on neighboring carbon atoms, up to 1–9, i.e., where the porphyrins are on opposite sides of the nanotube edge (**Figure 7**). The two most stable structures have been obtained for positions 1–4 and 1–6. In the 1–4 case, one porphyrin (in red) is adsorbed on the nanotube wall because of the flexibility of the $COOCH_2$-Ph linker. The second porphyrin (in blue) is partially inside the nanotube and the two molecules only weakly interact. In contrast, the porphyrins in the 1–6 system are oriented in such a way that they can directly interact, even though the distance and orientation of the cores are such that π–π interactions cannot take place (only CH-π interactions are present). Nevertheless, the 1–4 system is almost 20 kcal mol^{-1} more stable than its 1–6 counterpart; this is likely due to the strong favorable interaction between the "red" porphyrin molecule and the nanotube in the 1–4 model (Figure 7).

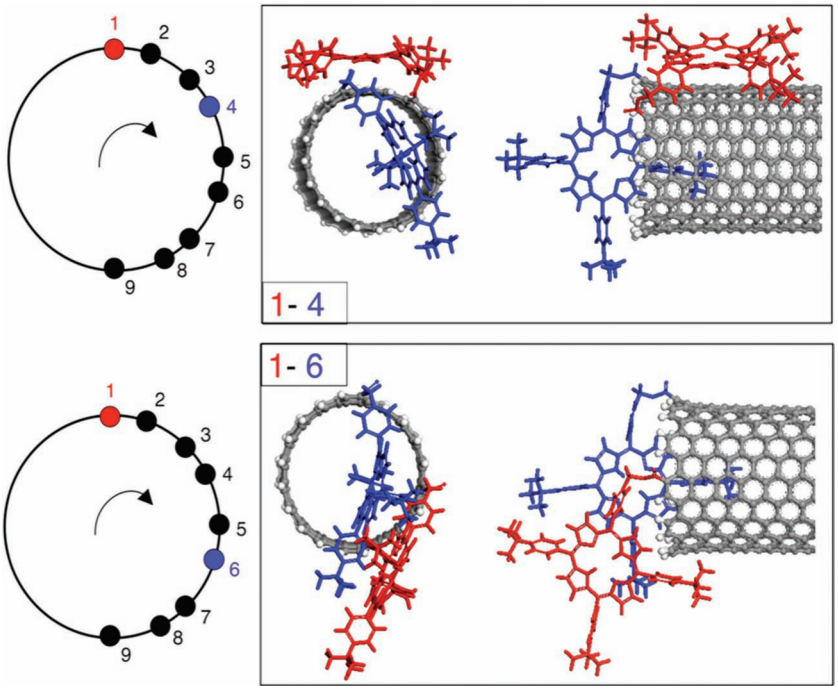

Figure 7. Front and side views for the 1–4 and 1–6 systems, in which two porphyrin molecules are attached at the nanotube tips.

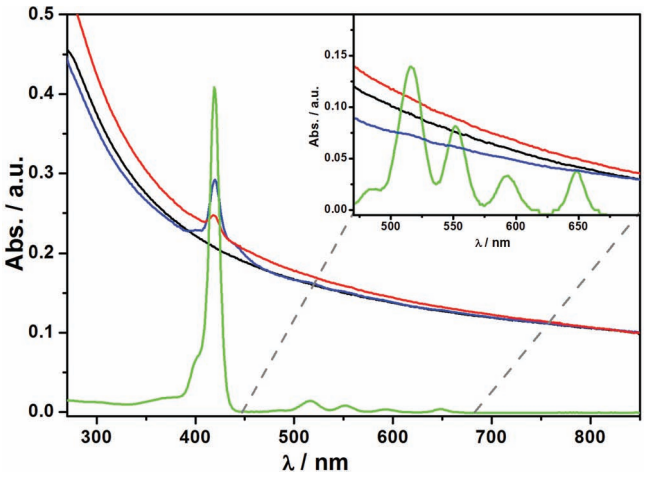

Figure 8. Electronic absorption spectra of **1** (green), ***ox*-DWCNTs** (black), **1-DWCNTs** (blue) and **1@DWCNTs** (red) in DMF. Inset: expanded Q-band region of all the materials. Spectra of DWCNTs materials are normalized at 850 nm.

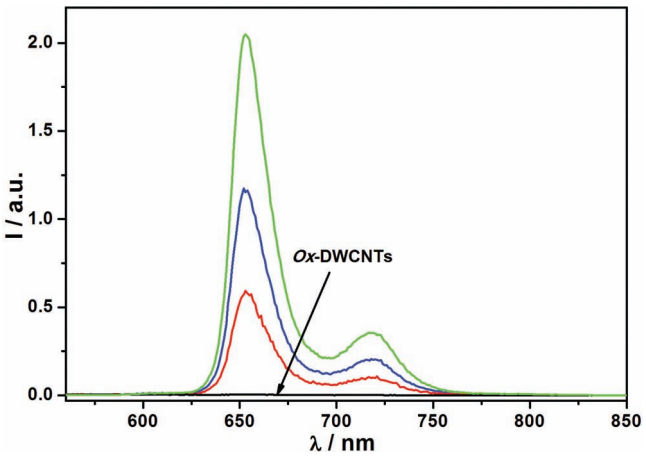

Figure 9. Emission spectra of **1** (green), ***ox*-DWCNTs** (black), **1-DWCNTs** (blue) and **1@DWCNTs** (red) upon excitation at 420 nm in DMF. Note: the qualitative trend of emission intensities is that observed experimentally (**1** > **1-DWCNTs** > **1@DWCNTs**) but the intensity ratios must not be taken for quantitative comparisons.

2.4. Photophysical Properties of Porphyrin-DWCNTs Derivatives

The photophysical studies of hybrid materials **1-DWCNTs** and **1@DWCNTs**, and reference samples **1** and ***ox*-DWCNTs** were carried out in DMF and $CHCl_3$, due to their proved efficacy in dispersing the carbon nanomaterials. The electronic absorption spectra of all the materials in DMF are shown in **Figure 8**. Both hybrid materials **1-DWCNTs** and **1@DWCNTs** show porphyrin-centered Soret bands at 419 nm, similar to free molecules **1**, whilst the weaker Q-bands are not discernible due to the overwhelming absorption of ***ox*-DWCNTs** counterpart. Similarly, Q-bands are barely observable in $CHCl_3$ dispersions along with the prominent Soret feature at 421 nm (Figure S10), Supporting Information. The different absorption intensities of the Soret band between the two hybrid materials reflect the higher porphyrin loading provided by covalent functionalization compared to the physisorbed **1@DWCNTs** sample. The broadening of the Soret band and a small shoulder around 450 nm suggest weak interporphyrin interactions, probably between those located on the same DWCNT unit (vide supra).[30] In addition, as suggested by molecular modeling, several conformations between the carbon nanotube surface and the porphyrin unit in solution may also result in broadening of the **1**-centered Soret band. Apart from the above changes, no other significant differences have been observed for the hybrid materials.[13,31]

The luminescence spectra of **1**, ***ox*-DWCNTs**, **1-DWCNTs** and **1@DWCNTs** were recorded using solutions with matching absorption at the Soret band maximum (420 nm). Upon excitation, the hybrid materials show a fluorescence profile that is perfectly superimposable to that of free porphyrin **1** in DMF (**Figure 9**) and $CHCl_3$ (Figure S11, Supporting Information). The emission intensities of **1-DWCNTs** and **1@DWCNTs** are found to be lower than that of porphyrin **1** alone, but a quantitative determination cannot be made due to at least four interfering factors (vide infra).[10,17,32] Therefore, this observation alone cannot be ultimately indicative of photoinduced energy or electron transfer processes causing quenching of the porphyrin singlet level.[17]

The observed reduction of the porphyrin fluorescence intensity of **1-DWCNTs** and **1@DWCNTs** may be due to factors such as i) light partitioning between **1** and DWCNTs, so that a considerable portion of the incoming photons causes excitation of the carbon nanotube scaffold; ii) excitation and emission light scattering due to the presence of particles in the hybrid dispersions, (vide supra); iii) different porphyrin concentration in the hybrid dispersions due to different functionalization methodology; and iv) significant presence of quenched "tight"-type conformers in which the porphyrins-centered singlet excited state is deactivated by the DWCNTs. Notably, the singlet excited state lifetime of the porphyrin is not reduced for all samples in both solvents (**Table 3**). This corroborates (i–iv) as reasonable explanations for the observed trends in luminescence intensities of Figure 9 and underpins the lack of evidence of photoinduced phenomena between porphyrins and DWCNTs. The porphyrin fluorescence decays of **1-DWCNTs** and **1@DWCNTs** are monoexponential, suggesting a uniform physical environment for the emissive centers in the dispersions. The slightly longer porphyrin lifetime value of the hybrid materials compared to free porphyrin can be caused by the reduced vibrational relaxation of the excited states of the porphyrin moieties when anchored on the rigid CNT walls.

Table 3. Singlet lifetime values of porphyrin **1** and hybrid materials in solution and PMMA matrix.

Sample	Lifetime [ns]		
	DMF	$CHCl_3$	PMMA
1	10.2	7.8	4.2
1-DWCNTs	10.6	8.9	4.4 (53%) 6.5 (47%)
1@DWCNTs	11.1	9.3	1.4 (50%) 8.1 (50%)
1@(1-DWCNTs)	9.9	–	–

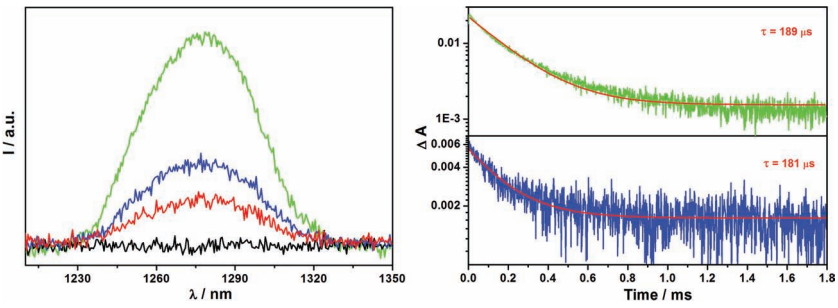

Figure 10. Sensitized singlet oxygen emission spectra (left) of **1** (green), ***ox*-DWCNTs** (black), **1-DWCNTs** (blue) and **1@DWCNTs** (red) by exciting at 420 nm in $CHCl_3$; the transient absorption decay curves (right) of **1** (green, O. D = 0.3, laser energy = 0.7 mJ per pulse) and **1-DWCNTs** (blue, O. D = 0.5, laser energy = 1.5 mJ per pulse), excited at 550 nm and collected at 470 nm.

To probe the triplet states of the appended porphyrins, experiments on sensitized singlet oxygen luminescence were carried out with **1**, **1-DWCNTs** and **1@DWCNTs** in $CHCl_3$.[33] Upon excitation of the porphyrin singlet bands, the lowest energy singlet state S_1 populates the lowest triplet state (T_1) through intersystem crossing. Owing to the long lifetime of porphyrin T_1, the molecular oxygen present in the solvent deactivates it through energy transfer and forms excited singlet oxygen ($^1O_2$), which emits at 1270 nm.[30] By monitoring the $^1O_2$ near infrared emission intensity, an indirect estimation of the triplet state generated by the porphyrins anchored on DWCNTs is obtained.[34] The $^1O_2$ emission bands from free porphyrin **1** and hybrid materials are shown in **Figure 10**. Due to the same reasons indicated for fluorescence spectra, singlet oxygen emission intensities of the hybrid materials are not directly comparable with that of porphyrin **1**.

In addition, porphyrin centered triplet state lifetimes of reference compound and hybrid materials were probed at 470 nm, using nanosecond transient absorption spectroscopy. The resulting decay curves are mono-exponentially fitted and the values are 189 μs and 181 μs for **1** and **1-DWCNTs**, respectively (Figure 10).[35] Identical triplet lifetimes confirm the presence of unquenched porphyrin units in the hybrid material. Unfortunately, we could not detect any dynamic processes attributable to transient species such as the notoriously-weak features of the radical porphyrin-centered cations or nanotube-centered anions most probably due to the strong background signals deriving from the porphyrin singlet and triplet transient absorption bands. In addition, as outlined above in DLS section, the size of the CNT-porphyrin hybrids causes strong scattering of excitation light further limiting the goodness and sensitivity of the transient absorption measurements.

As discussed above, molecular modeling suggests the existence of "loose" and "tight" pairs between porphyrins and DWCNTs. Unlike the case of the fullerene systems,[28,30] the photophysical analysis cannot provide direct evidence for such interchromophoric interactions, but anyway do not contradict such model. In fact, if the fluorophore and the quencher are approaching each other up to the shortest distance ("tight" conformation), photo-induced energy/electron transfer rates may become so fast to successfully compete with the intrinsic deactivation of the porphyrin and yield complete quenching of luminescence. In other words, this "tight" situation must lead to a virtually complete reduction of the emission intensity and a vanishingly short lifetime. On the other hand, in the case of "loose" pairs, the attached chromophores should behave as in the absence of quenching interactions and must show the characteristic luminescence properties of **1**. Hence, luminescence data are compatible with the presence of "tight" and "loose" pairs, with the latter being responsible for the residual and kinetically unquenched luminescence signals. This picture of non-interacting porphyrin/DWCNTs arrangements is supported by the observation of singlet oxygen luminescence that further signals the presence of completely unquenched porphyrin moieties in their triplet states. These findings are somewhat surprising since those indicate the absence of intermediate situations, in between "tight" and "loose", where the porphyrin-DWCNTs distance causes dynamic quenching of the porphyrin moieties with reduced singlet lifetimes.

Finally, DMF dispersions of **1@(1-DWCNTs)** were also investigated. The absorption and emission features of **1@(1-DWCNTs)** exhibit an intensity quite similar to **1**, showing the high loading of porphyrins on DWCNTs (Figure S12, Supporting Information). Similarly to **1-DWCNTs** and **1@DWCNTs**, no shift or broadening is observed either in absorption or in emission bands. Also the lifetime value (τ = 9.9 ns) exactly matches with that of porphyrin **1** alone, suggesting a similar situation as observed in $CHCl_3$.

To shed further light on the electronic properties of **1-DWCNT** and **1@DWCNTs** incorporated in polymeric active layers, thin films have been prepared by dispersing the hybrid materials in the pyrene-terminated poly(3-hexylthiophene) polymer, P3HT-Py (see preparation protocols in the Supporting Information). The dispersions were spin coated on a indium tin oxide (ITO) glass surface, but the overwhelming spectral features of the P3HT-Py matrix hid all the absorption and emission bands of the porphyrin, thus hampering the photophysical characterization of the hybrid materials in this medium (Figure S13, Supporting Information). Therefore, in order to investigate the optical properties of the DWCNTs hybrids in a polymer matrix, the transparent and photo-inactive poly(methylmethacrylate) (PMMA) polymer was chosen as the solid-state medium and related thin films were made by drop-casting $CHCl_3$ dispersions containing all the conjugates. In contrast to solution experiments, the spectral features of **1**, **1-DWCNTs** and **1@DWCNTs** recorded in PMMA thin films show the presence of aggregates (**Figure 11**). For molecule **1**, the split Soret band and the red-shifted Q-band maximum are indicative of *J*-type "head-to-tail" porphyrin aggregation.[13,36,37] The formation of *J*-aggregates is promoted by the poor porphyrin dispersibility in aliphatic PMMA polymer and by the presence of dipoles induced by polar -OH functionality on the macrocyclic rings. According to Kasha's theory, these large structures substantially modify the pattern of the Soret (splitting) and Q-bands (red-shifted maximum), as indeed observed here.[38] Interestingly, the same spectral features of **1** alone are

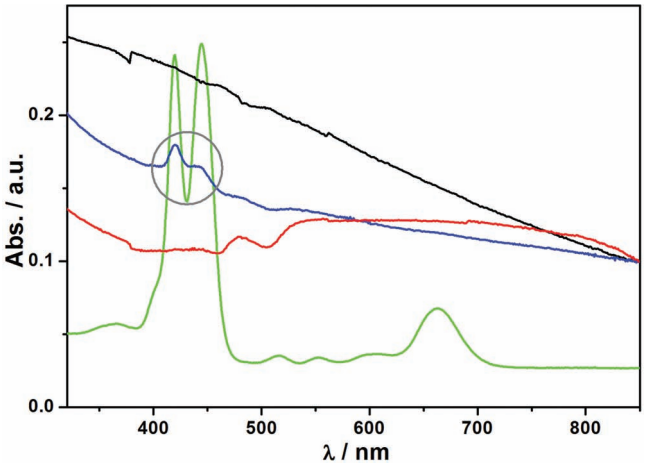

Figure 11. Electronic absorption spectra of **1** (green), ***ox*-DWCNTs** (black), **1-DWCNTs** (blue) and **1@DWCNTs** (red) in PMMA polymer matrix.

observed in the PMMA dispersion of **1-DWCNTs**, suggesting a similar ordered arrangement of the porphyrin chromophores in the rigid medium. Such *J*-type interactions are perhaps favored by steric effects induced by the presence of the highly hindered DWCNTs framework, whereas face-to-face intramolecular interactions seem to be prevented, as also confirmed by the absorption spectra obtained from solution (vide supra).[39] For samples containing **1@DWCNTs**, owing to the low concentration of porphyrins, the related electronic absorption bands are masked by the strong absorption of DWCNTs. However, luminescence measurements (λ_{exc} = 420 nm) show a weak band clearly attributable to porphyrin fluorescence, thus confirming the presence of the chromophore in the sample (Figure S14, Supporting Information). Upon excitation of **1@DWCNTs** at 445 nm, a broader fluorescence band is detected (**Figure 12**), and the related excitation spectrum collected at the emission maximum showing a split Soret band, where the new feature is higher in energy (395 nm) than the characteristic band at 419 nm. Compared to **1** and **1-DWCNTs**, these findings suggest a different arrangement of the porphyrin units in **1@DWCNTs**, i.e., face-to-face *H*-aggregates, which are not generated in **1-DWCNTs** as discussed above.[37] The allowed in-phase arrangement of transition dipoles in *H*-aggregates results in a higher energy electronic transition which is responsible for the Soret band peak at shorter wavelength.

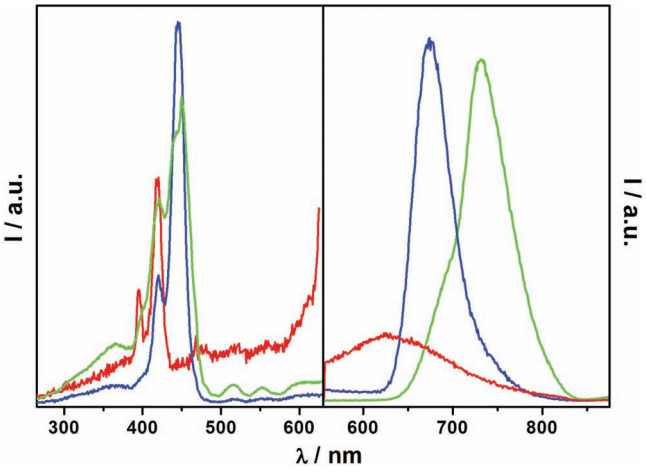

Figure 12. Excitation (left) and emission (right, λ_{em} = 445 nm) spectra of **1** (green), **1-DWCNTs** (blue) and **1@DWCNTs** (red) in PMMA polymer matrix. The excitation spectrum of each material is collected at its respective emission maximum.

On the other hand, the out-of-phase arrangement of transition dipoles generates a forbidden, low energy, transition to the S_1 state. Upon excitation of **1@DWCNTs**, the high energy S_2 level is populated, which then decays to a weakly emitting S_1 state.[37] In *J*-aggregates, depending on the strength of interchromophoric interaction, the low energy exciton states shift the emission maxima accordingly, i.e., the stronger the interaction the more red-shifted the band is. The emission spectra of **1** and **1-DWCNTs** exhibit maxima at 732 and 675 nm respectively, indicating stronger interactions in the aggregates of **1** alone than in those of the more sterically congested **1-DWCNTs** (λ_{exc} = 445 nm, Figure 12).[37] Apart from the presence of *J* and *H* aggregates, characteristic porphyrin-centered emission bands are still observed in all three materials when exciting the Soret (420 nm) and Q band (515 nm) features (Figure S14, Supporting Information). This shows the presence of free porphyrin units, especially in the case of hybrid materials, where the porphyrin emission intensity is significantly high. The fluorescence decay profiles of **1-DWCNTs** and **1@DWCNTs**, which are fitted as biexponential, support the above rationale. Both hybrid materials possess a long and a short lifetime with a similar proportion (Table 3). Notably, the short lifetime of **1-DWCNTs** is the same as that of **1**, confirming similar aggregation processes in both materials. The long lifetime stems from non-aggregated porphyrin units as evidenced by the emission spectrum. In **1@DWCNTs**, as mentioned above, the excited S_1 state rapidly decays to the ground state (τ = 1.4 ns). Similar to the solution phase, the physisorbed porphyrins show a longer lifetime value than that of the free porphryrins. This is attributed to the reduced vibrational relaxation from the lower-lying excited state (Table 3), ultimately confirming their interaction with the DWCNTs framework.

2.5. Optoelectronic Characterization of Porphyrin-DWCNTs Blends into Polythiophenes-Based Polymers for Photovoltaic Applications

The role of the functionalized CNTs frameworks in the polymer blends for photovoltaic applications is subtle as they could behave like versatile, interpenetrating unidimensional hole-extracting materials as well as electron accepting units and conductive networks.[15,40,41] Therefore, in order to evaluate the potential properties of the porphyrin-DWCNTs derivatives in PV devices, we fabricated several glass/ITO/PEDOT:PSS/active layer/Al devices with the aim of investigating the interaction of the chemically-modified DWCNTs and of **1@(1-DWCNTs)** with the P3HT-Py polymer matrices by addressing the reproducibility of both morphological and conducting properties of the active layers. Besides small concentrations of the DWCNT derivatives (*ca.* 1%), we also added small amounts of [60] PCBM (<5%) in order to balance the charge carrier transport to the electrodes. Specifically, 100-nm thin films were prepared

by spin-coating a solution (c = 15 mg mL^{-1}) of *p*-xylene containing the appropriate amounts of derivatized DWCNTs, [60]PCBM and P3HT-Py.

Scanning near-field optical microscopy AFM (AFM-SNOM) studies have been carried out to study the morphology of the thin films containing the active layers from composite dispersions of the porphyrin-based DWCNTs investigated in this work.[42] The results are shown in **Figure 13**b. The typical topography of the thin films containing **1@(1-DWCNTs)** is presented at micro-scale in the left panel and the SNOM signal (accumulated in the transmission mode) is displayed in the right panel. Both images clearly show a region where the functionalized DWCNTs are debundled and in intimate contact with the P3HT-Py polymer, as also highlighted by the uniform distribution of the tubes within the polymeric layer. At these low-doping levels, the porphyrin-DWCNT hybrids do not protrude from the film and their UV-Vis absorption is much smaller than that of the surrounding polymer matrix. In addition, the intrinsic UV-Vis absorption properties of the porphyrin fragments at the working wavelength (i.e., 532 nm) do not seem to noticeably influence the optical contrast imaging of the functionalized DWCNTs and PCBM. On the other hand, the presence of dark spots in the SNOM image is attributed to zones of the layer in which [60]PCBM molecules are aggregated.[42]

Figure 13a presents the room-temperature dark current density-voltage (J–V) characteristics of typical P3HT-Py films containing the carbon nanohybrid structures. The forward bias conditions correspond to positive voltage on the ITO electrode with respect to the Al cathode. The J–V dependence is asymmetric, suggesting the presence of a blocking contact (Schottky barrier) at the bottom of the poly(3,4-ethylenedioxythiophene): poly(styrenesulfonate) PEDOT:PSS/active layer interface. This is responsible for the observed rectification effect as the other upper interface is supposed to behave like an Ohmic contact. At high voltages, the series resistance or the space charge build up deviates the injected current from the exponential behavior limit. Thus, the observed intensification of the forward current in the **1@(1-DWCNTs)**-based devices suggests a smaller hole-injection barrier compared to those reference devices containing ***p***-MWCNTs. Our results corroborate state-of-the-art works[41] and the standard metal-insulator-metal model, where the built-in potential across the organic thin film equals the work function difference between the Al cathode (4.3 eV) and the PEDOT:PSS anode (5.1 eV), providing a distinctive kink structure in the forward bias of the J–V plots. The increase in the forward current observed for films containing hybrids **1@(1-DWCNTs)** is accompanied by a better rectification ratio compared to the responses displayed by devices containing ***p*-DWCNTs** and ***ox*-DWCNTs** where a very similar behavior, with minor differences in the low bias regime, has been observed. In order to evaluate the photoactive role of the porphyrin moieties within the active layer, quantum efficiency measurements have been performed. In particular, an experimentally accessible value is the external quantum efficiency or incident photon to current efficiency (EQE), which is defined as the number of photogenerated charge carriers over the number of incident monochromatic photons. In this respect, the lineshape of the EQE profile (in arb. units), normalized at 420 nm, is displayed in the inset of Figure 13a and closely follows the absorption band of the polymer blend. No differences have been detected between active layers containing the porphyrin-functionalized hybrid or reference CNTs, thus indicating a negligible effect of the porphyrin moieties.

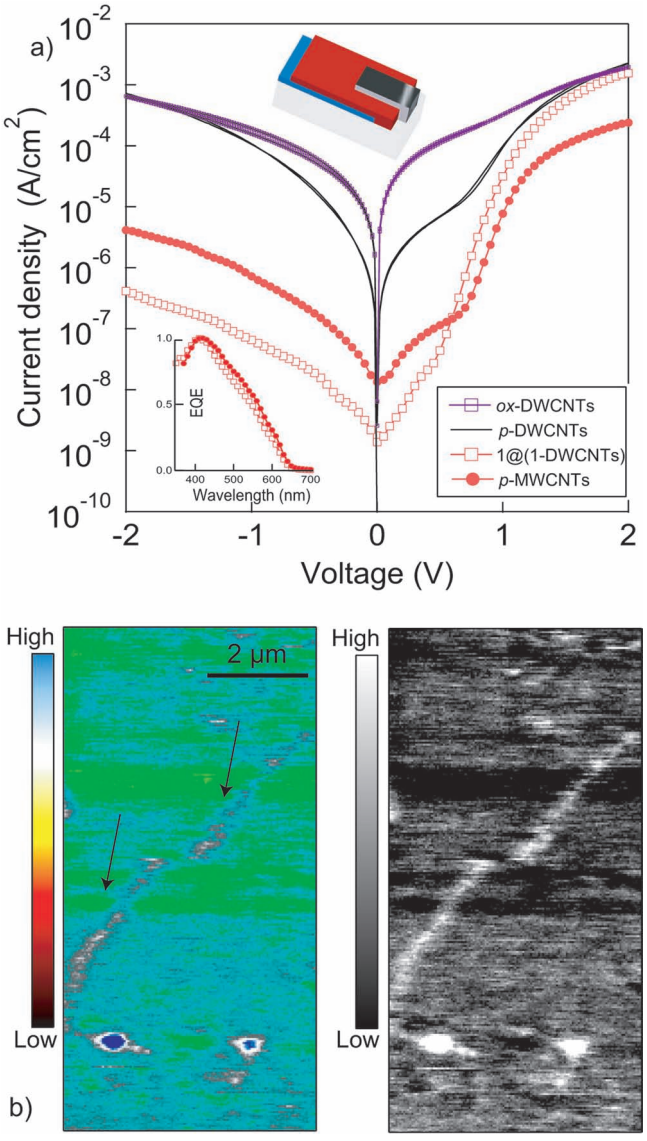

Figure 13. a) J–V curves measured in dark, at room temperature, for thin films of P3HT-Py loaded with reference *p*-MWCNTs and PCBM (filled circles), with ***p*-DWCNTs** and PCPM (black curve), with ***ox*-DWCNTs** and PCBM (blue curve) and doped with **1@(1-DWCNTs)** and PCBM (empty squares). The device structure (glass/ITO/PEDOT:PSS/active layer/Al) is schematically shown. Inset: Normalized EQE wavelength dependencies for fabricated thin films with ***p***-MWCNTs and porphyrin-functionalized DWCNTs; b) coupled AFM topography (left) and SNOM optical contrast (right) microscopy images obtained under monochromatic laser radiation (532 nm) for the as-deposited active layers including **1@(1-DWCNTs)**. At the bottom of the images, protrusions in the film are observed (several tenths of nanometers above the surface in the AFM panel), which can be associated to **1@(1-DWCNTs)** surrounded by PCBM and/or porphyrin aggregates in the SNOM transmission image.

3. Conclusions

Aiming at the understating of the role of CNTs dopants in active layers of OPV systems in this work we have reported the preparation and physical characterization of diverse porphyrin-derived DWCNTs conjugates. In particular, COOH-derived DWCNTs, produced by means of a three-step oxidative protocol, have been covalently linked and physically absorbed to a free-base porphyrin molecule. The photophysical properties of the porphyrin-DWCNTs derivatives have been investigated through absorption and emission spectroscopies both in solution and in the solid state. In particular, as previously observed for fullerene-porphyrin dyads, we hypothesized that the luminescence data are compatible with the presence of "tight" and "loose" pairs, with the latter being responsible for the intensive residual and kinetically unquenched luminescence signals. Therefore, contrary to previous literature reports, definitive experimental evidence could not be obtained with our materials to support photoinduced electron and/or energy transfer processes involving the porphyrin chromophores and the nanotube framework. On the other hands, asymmetric current density–voltage profiles of typical films containing P3HT-Py polymer doped with small amounts of [60]PCBM and porphyrin-DWCNTs derivatives displayed dramatic rectification effects in line with state-of-the-art literature devices. Notably, this effect is clearly evident in the forward current for the porphyrin-DWCNT-doped films if compared to those responses deriving from active layers solely containing ***p*-DWCNTs** and ***ox*-DWCNTs**, thus ultimately confirming the key role of the porphyrin scaffold. On the other hand, external quantum efficiency measurements normalized at 420 nm suggested that the porphyrin-centered photophysical properties have a null effect on the device performances. Taken all together, these observations provide strong evidences of a structural rather than a photoactive role of the porphyrin moieties on the device electrical conductivity, possibly originating from favorable *H*- type aggregations as observed in the solid state by steady-state UV-Vis absorption and fluorescence spectroscopies. In particular, the significant amount of porphyrin loading, namely the additional layer of molecules for samples containing **1@(1-DWCNTs)** is thought to favor the dispersion of the hybrid materials in the polymeric matrix and the formation of aggregates that ultimately control the morphology, miscibility, and alignment of functionalized CNTs in the device active layer.

Current investigations are now aimed at the engineering a next-generation of porphyrin-acceptors-DWCNTs hybrids in which photo-induced charge separation and the carrier transport in porphyrin-functionalized DWCNTs composites based on P3HT-Py may be further improved by inserting PCBM-like moieties between the porphyrin macrocycle and the DWCNTs external wall.

4. Experimental Section

Technical and experimental (XPS, IR, TGA, TEM, AFM, DLS, UV-Vis and emission spectroscopies and *J–V* characteristics) details are reported in the Supporting Information.

Synthetic Procedures: 5,10,15-Tris-(4-*tert*-butylphenyl)-20-(4-hydroxybenzyl)porphyrin, **1**: To a solution of methyl ester-porphyrin **2** (740 mg, 1.02 mmol) in dried THF (74 mL), $LiAlH_4$ (77.4 mg, 2.04 mmol) was added under argon at 0 °C and the solution was stirred for 1 h. The mixture was then allowed to warm to r.t. and quenched with Et_2O. Subsequently, the mixture was washed with acidified H_2O, dried over $MgSO_4$ and the solvent removed in vacuo. The crude was then purified by silica gel chromatography (eluent: CH_2Cl_2) and by precipitation from CH_2Cl_2/MeOH, yielding porphyrin **1** (500 mg, 70%) as a purple solid. M.p. > 300 °C; ^{1}H-NMR (400 MHz, $CDCl_3$, δ): 8.87 (m, 6H, Pyrrole), 8.82 (m, 2H, Pyrrole), 8.22 (d, *J* 7.8, 2H, Ar-*H*), 8.14 (m, 6H, Ar-*H*), 7.76 (d, *J* 7.8, 8H, Ar-*H*), 5.07 (d, 2H, CH_2), 1.97 (s broad, 1H, O*H*), 1.61 (s, 27H, C(CH_3)$_3$), (Pyrrole-NH not visible); ^{13}C-NMR (100 MHz, $CDCl_3$, δ): 150.47, 141.71, 140.09, 139.14, 134.79, 134.49, 134.45, 131.03, 125.27, 123.59, 120.34, 120.22, 119.35, 65.44, 34.88, 31.68; IR(cm^{-1}): ν 3416.3, 3317.9, 3027.2, 2956.4, 2864.2, 2359.9, 1556.2, 1501.9, 1473.5, 1397.3, 1348.9, 1266.4, 1221.7, 1185.9, 1107.5, 1020.6, 981.9, 966.8, 879.9, 848.4, 732.7, 577.5, 456.2, 426.7, 413.9; MALDI-HRMS: Found 812.4451 [(M^+), $C_{57}H_{56}N_4O^+$] requires 812.4454; UV-Vis (CH_2Cl_2, 25 °C): λ_{max} (ε mol^{-1} L cm^{-1}) = 419 (630808), 517 (15342), 552 (5926), 592 (848). ***ox*-DWCNTs**: ***p*-DWCNTs** (200 mg, Nanocyl 2100, lot n° 080526) were sonicated for 5 min in a 200 mL H_2O_2 15% solution, and then heated at 100 °C for 3 h. The resulting suspension was then poured in H_2O (1 L) and then filtered through a 0.4 μm polycarbonate filter. The black precipitate was washed several times with 200 mL of H_2O, and then with few mL of MeOH to ease the drying under reduced pressure. The same procedure was repeated other two times. Thus, starting with an overall amount of 600 mg of ***p*-DWCNTs**, 252 mg of a black powder were collected. The product was then dispersed in 50 mL of a 2N HCl solution through 5 min of sonication and then stirred at r.t. for additional 10 min. The resulting suspension was then filtered through 0.4 μm polycarbonate filters allowing the collection of a black precipitate. Heating at 450 °C under air for 45 min afforded 175 mg of oxidized material, which was subsequently dispersed in 200 mL of a 3:1 H_2SO_4 (95%) HNO_3 (65%) aqueous solutions through 2 min of sonication. The resulting black dispersion was stirred at r.t. for 1 h. The reaction mixture was then poured into 1 L of H_2O and then filtered through 0.4 μm polycarbonate filters. The black precipitate was again washed several times with 200 mL of H_2O, and then with few mL of MeOH. After this step, 134 mg of material were collected (overall yield = 22% w/w). **1-DWCNTs**: 50 mg of ***ox*-DWCNTs** were dispersed in 10 mL of DMF through continuous sonication. After 20 min, 1 mL of pyridine and hydroxy-benzotriazole (HOBt, 100 mg, 750 μmol) were sequentially added to the dispersion. After 35 min and 50 min of sonication, EDC (88 mg, 540 μmol) and a solution of **1** (100 mg, 122 μmol) in 5 mL of DMF were respectively added. The reaction mixture was sonicated for further 30 min and then stirred at r.t. for 48 h. The resulting dispersion was precipitated in H_2O (100 mL) and then filtered through 0.4 μm polycarbonate filter. The black powder was then washed with small additions of H_2O (200 mL) and MeOH to ease the drying under reduced pressure. The precipitate was then dispersed in 5 mL of DMF, precipitated in $CHCl_3$ (100 mL) and then filtered through 0.45 μm polytetrafluoroethylene filter. The dispersion/precipitation in $CHCl_3$ was repeated 5 times, until the filtered solution was completely colorless. The complete discard of unreacted porphyrins was also confirmed by UV-Vis spectroscopic analysis. 43 mg of black material were collected. **1@(1-DWCNTs)**: 30 mg of ***ox*-DWCNTs** were dispersed in 5 mL of DMF under sonication and after 10 min 500 μL of pyridine were added. After 20 min and 35 min of continuous sonication, *N*-hydroxysuccinimide (NHS, 100.3 mg, 854 μmol) and EDC (88 mg, 540 μmol) were sequentially added. After 45 min of sonication, a solution of **1** (80 mg, 98 μmol) in 5 mL of DMF was added. The reaction mixture was sonicated for further 30 min and then stirred at r.t. for 48 h. The reaction mixture was then precipitated in 200 mL of H_2O and the resulting black-violet suspension was filtered through 0.2 μm polycarbonate filter. The black precipitate was washed through small additions of H_2O (200 mL) and then with acetone (400 mL). The precipitate was then dispersed in 5 mL of DMF, precipitated in acetone (200 mL) and then filtered through 0.45 μm polytetrafluoroethylene filter. 25 mg of black material were then collected. **1@DWCNTs**: 50 mg of *sh*-DWCNTs were dispersed in 10 mL DMF through continuous sonication. After 20 min 1 mL of pyridine and HOBt (100 mg, 750 μmol) were sequentially added. After 50 min of sonication a solution of **1** (100 mg, 122 μmol) in 5 mL of DMF was added. The reaction mixture was sonicated for further 30 min and then stirred at r.t. for 48 h. The resulting dispersion was precipitated

in H_2O (100 mL) and then filtered through 0.4 μm polycarbonate filter. The powder was washed with small additions of H_2O (200 mL) and then MeOH to ease the drying under reduced pressure. The precipitate was then dispersed in 5 mL of DMF, precipitated in $CHCl_3$ (100 mL) and then filtered through 0.45 μm polytetrafluoroethylene filter. The dispersion/precipitation in $CHCl_3$ was repeated 5 times, until the filtered solution was completely colorless. The complete discard of unreacted porphyrins was also confirmed by UV-Vis spectroscopic analysis. 40 mg of black material were then collected.

Molecular Modeling: The simulations have been performed with the molecular modeling package Material Studio 5.0 and its implementation of the Dreiding force field has been used. All simulations have been performed in vacuum in the NVT (constant number of particles, volume and temperature) ensemble at room temperature and are 5 ns long, with a time step of 1 fs. To maintain the computational effort to a reasonable level, a 5.4 nm long non-periodic, single-walled armchair (10,10) carbon nanotube (SCWNT) was used.

Photophysical Studies: Solution: Approximately 0.5 mg of each DWCNTs derivative was dispersed in 3 mL of DMF or $CHCl_3$ solvent by sonicating for 5 min. 1 mL of each dispersion was filtered through cotton to avoid visible floating materials, and diluted to 2 mL with DMF or chloroform solvent. The resulted optically transparent solutions were used for the DLS and photophysical measurements. Transient absorption spectra were obtained by using the nanosecond flash photolysis apparatus Proteus by Ultrafast Systems LLC. Triplet lifetimes were obtained by averaging 132 or 254 different decays recorded around the maximum of the absorption peak (470 nm). The samples were placed in fluorimetric 1 cm path cuvettes and purged from oxygen by at least 4 freeze–thaw–pump cycles. Details on the experimental apparatus are described elsewhere.[28] *PMMA Matrix:* Approximately 1 weight% (wt%) of each DWCNTs derivative (0.5 wt% of porphyrin, to avoid concentration dependent aggregation) was dispersed in 3 mL of PMMA/$CHCl_3$ solution and sonicated for 10 min. This solution was drop-casted on clean optical glass plates and left over night to dry $CHCl_3$. The resulting transparent thin films were used for the photophysical studies. *P3HT-Py Matrix:* Approximately 1 wt% of each DWCNTs derivative and porphyrin, 5 wt% of PCBM, 94 wt% of P3HT-Py (Mn: 11 K g mol^{-1}, PDI 1.2) were dissolved or dispersed in *o*-dichlorobenzene (20 mg mL^{-1}) by sonication for 90 min and left for overnight stirring. Approximately 200 μL of each solution were then spin coated (1000 rpm, 90 s) on clean ITO/glass surfaces. Further, the spin coated glasses are allowed to dry naturally and then used for the photophysical studies.

Device Fabrication: The anode was patterned by wet etching of 100 nm thick ITO-coated glass, commercially available from Praezisions Glass und Optik (CEC020S). The cleaning of the substrates, prior to the precoating with 50 nm of PEDOT:PSS and deposition of the active layers, consisted in ultrasonication in acetone and rinsing in *i*PrOH and deionized water. As received PEDOT:PSS solution (Baytron P VPAI 4083 from H. C. Starck) was passed through 0.20 μm filters and spin-coated on ITO (1000 rpm s^{-1}, 6000 rpm, 60 s). The substrates were then baked 20 min at 135 °C in air. Preparation of the active layers was performed following standard procedures. Briefly, PCBM was purchased from Sigma-Aldrich and used as received. For the series of devices presented here, *p*-xylene (HPLC grade) was used as a solvent and composite dispersions were obtained by combining an appropriate mass of carbon nanotubes with PCBM and P3HT-Py (Mn: 11 K g mol^{-1}, PDI 1.2) at desired doping levels. Thin films were spin-coated from solutions with ca. 15 mg mL^{-1} concentration. All solutions were ultrasonicated for 90 min at 50 °C (Branson 2510) and gently stirred for at least 12 h at r.t. before spin coating (1000 rpm s^{-1}, 1000 rpm, 90 s). The spin coating step occurred in a glovebox at room temperature. The thicknesses of the fabricated devices were around 100 nm. The structures were dried, annealed for 30 min at 135 °C in nitrogen and kept 4 h under vacuum. For electrical characterization, an Al top contact (ca. 80 nm thick) was thermally evaporated through a shadow mask to complete the structures and the samples were maintained at room temperature during the deposition. The effective working areas of the investigated structures were in the range 0.04–1 cm^2 and were measured with an optical microscope.

Supporting Information

Supporting Information is available from the Wiley Online Library or from the author.

Acknowledgements

The Namur-Mons-Louvain collaboration, Belgium, was supported by the SOLWATT program of Région Wallonne (SUNTUBE projet). The work in Namur was also supported by the EU (ITN "FINELUMEN" PITN-GA-2008-215399), FNRS (FRFC contracts n° 2.4.550.09 and 2.4.617.07.F and MIS n° F.4.505.10.F), the 'TINTIN' ARC project (contract n° 09/14-023), the Loterie Nationale and the University of Namur (internal funding). The work in Mons was supported by the Belgian Federal Office for Science Policy BELSPO (IAP 6/27), Région Wallonne (Programme d'Excellence OPTI2MAT) and FNRS-FRFC. In Bologna, Italy, the work was supported by EU (ITN "FINELUMEN" PITN-GA-2008-215399) and the CNR (PM.P04.010, MACOL). N.A. thanks Dr. Enrico Rampazzo, University of Bologna, for the help with DLS measurements. The work in Louvain-la-Neuve, Belgium, was supported by the TINTIN project–ARC, Communauté Française de Belgique, and the Belgian National Fund for Scientific Research (FRS-FNRS) via the F.4501.05 grant and FRFC projects 2.4546.08, 2.4505.09 and 2.4510.11. S.M. is a FRS-FNRS research fellow. V.C. thanks the University of Trieste for her PhD fellowship. R.M. acknowledges generous funding from the FNRS for his postdoctoral fellowship. C.A. thanks Pier Luigi Cerasoli for artwork support.

Received: November 2, 2011
Revised: February 9, 2012
Published online: May 3, 2012

[1] N. Armaroli, V. Balzani, *Energy for a Substainable World. From the Oil to a Sun Powered Future*. Wiley-VCH, Weinheim **2011**.
[2] N. Armaroli, V. Balzani, *Energ. Environ. Sci.* **2011**, *4*, 3193.
[3] a) M. Granstrom, K. Petritsch, A. C. Arias, A. Lux, M. R. Andersson, R. H. Friend, *Nature* **1998**, *395*, 257; b) J. J. M. Halls, C. A. Walsh, N. C. Greenham, E. A. Marseglia, R. H. Friend, S. C. Moratti, A. B. Holmes, *Nature* **1995**, *376*, 498.
[4] J.-L. Bredas, J. R. Durrant, *Acc. Chem. Res.* **2009**, *42*, 1689.
[5] a) Heliatek organic based photovoltaics, http://www.heliatek.com, (accessed November 2011); b) Plastic Solar Panels by Solarmer, http://www.solarmer.com, (accessed November 2011)
[6] a) G. C. Bazan, J. Peet, J. Y. Kim, N. E. Coates, W. L. Ma, D. Moses, A. J. Heeger, *Nat. Mater.* **2007**, *6*, 497; b) C. N. Hoth, P. Schilinsky, S. A. Choulis, C. J. Brabec, *Nano Lett.* **2008**, *8*, 2806; c) K. Vandewal, K. Tvingstedt, A. Gadisa, O. Inganas, J. V. Manca, *Nat. Mater.* **2009**, *8*, 904.
[7] a) D. M. Guldi, G. M. A. Rahman, V. Sgobba, C. Ehli, *Chem. Soc. Rev.* **2006**, *35*, 471; b) V. Sgobba, D. M. Guldi, *Chem. Soc. Rev.* **2009**, *38*, 165; c) V. Sgobba, G. M. A. Rahman, D. M. Guldi, *Carbon Nanotubes in Electron Donor-Acceptor Nanocomposites - Chemistry of Carbon Nanotubes*, American Scientific Publishers, Valencia, CA **2007**; d) R. C. Haddon, *Acc. Chem. Res.* **2002**, *35*, 997.
[8] a) R. H. Baughman, A. A. Zakhidov, W. A. de Heer, *Science* **2002**, *297*, 787; b) T. W. Ebbesen, H. J. Lezec, H. Hiura, J. W. Bennett, H. F. Ghaemi, T. Thio, *Nature* **1996**, *382*, 54; c) A. A. Mamedov, N. A. Kotov, M. Prato, D. M. Guldi, J. P. Wicksted, A. Hirsch, *Nat. Mater.* **2002**, *1*, 257; d) C. Q. Sun, H. L. Bai, B. K. Tay, S. Li, E. Y. Jiang, *J. Phys. Chem. B* **2003**, *107*, 7544.
[9] M. A. Green, K. Emery, Y. Hishikawa, W. Warta, *Prog. Photovoltaics* **2011**, *19*, 84.
[10] D. Baskaran, J. W. Mays, X. P. Zhang, M. S. Bratcher, *J. Am. Chem. Soc.* **2005**, *127*, 6916.

[11] a) S. Campidelli, C. Sooambar, E. L. Diz, C. Ehli, D. M. Guldi, M. Prato, *J. Am. Chem. Soc.* **2006**, *128*, 12544; b) Z. B. Liu, J. G. Tian, Z. Guo, D. M. Ren, T. Du, J. Y. Zheng, Y. S. Chen, *Adv. Mater.* **2008**, *20*, 511; c) T. Palacin, H. Le Khanh, B. Jousselme, P. Jegou, A. Filoramo, C. Ehli, D. M. Guldi, S. Campidelli, *J. Am. Chem. Soc.* **2009**, *131*, 15394.

[12] J. Jin, Z. P. Dong, J. G. He, R. Li, J. T. Ma, *Nanoscale Res. Lett.* **2009**, *4*, 578.

[13] H. Li, R. B. Martin, B. A. Harruff, R. A. Carino, L. F. Allard, Y. P. Sun, *Adv. Mater.* **2004**, *16*, 896.

[14] a) J. Y. Chen, C. P. Collier, *J. Phys. Chem. B* **2005**, *109*, 7605; b) F. Y. Cheng, S. Zhang, A. Adronov, L. Echegoyen, F. Diederich, *Chem. Eur. J.* **2006**, *12*, 6062; c) K. S. Chichak, A. Star, M. V. R. Altoe, J. F. Stoddart, *Small* **2005**, *1*, 452; d) R. Chitta, A. S. D. Sandanayaka, A. L. Schumacher, L. D'Souza, Y. Araki, O. Ito, F. D'Souza, *J. Phys. Chem. C* **2007**, *111*, 6947; e) C. Ehli, G. M. A. Rahman, N. Jux, D. Balbinot, D. M. Guldi, F. Paolucci, M. Marcaccio, D. Paolucci, M. Melle-Franco, F. Zerbetto, S. Campidelli, M. Prato, *J. Am. Chem. Soc.* **2006**, *128*, 11222; f) H. P. Li, B. Zhou, Y. Lin, L. R. Gu, W. Wang, K. A. S. Fernando, S. Kumar, L. F. Allard, Y. P. Sun, *J. Am. Chem. Soc.* **2004**, *126*, 1014; g) H. Murakami, T. Nomura, N. Nakashima, *Chem. Phys. Lett.* **2003**, *378*, 481; h) J. K. Sprafke, S. D. Stranks, J. H. Warner, R. J. Nicholas, H. L. Anderson, *Angew. Chem. Int. Ed.* **2011**, *50*, 2313.

[15] D. M. Guldi, G. M. A. Rahman, M. Prato, N. Jux, S. H. Qin, W. Ford, *Angew. Chem. Int. Ed.* **2005**, *44*, 2015.

[16] T. Hasobe, S. Fukuzumi, P. V. Kamat, *J. Am. Chem. Soc.* **2005**, *127*, 11884.

[17] G. M. A. Rahman, D. M. Guldi, S. Campidelli, M. Prato, *J. Mater. Chem.* **2006**, *16*, 62.

[18] a) D. Tasis, N. Tagmatarchis, A. Bianco, M. Prato, *Chem. Rev.* **2006**, *106*, 1105; b) J. L. Delgado, M. A. Herranz, N. Martin, *J. Mater. Chem.* **2008**, *18*, 1417; c) A. Hirsch, *Angew. Chem. Int. Ed.* **2002**, *41*, 1853; d) P. Singh, S. Campidelli, S. Giordani, D. Bonifazi, A. Bianco, M. Prato, *Chem. Soc. Rev.* **2009**, *38*, 2214.

[19] H. Imahori, S. Fukuzumi, *Adv. Funct. Mater.* **2004**, *14*, 525.

[20] a) D. M. Guldi, *J. Phys. Chem. B* **2005**, *109*, 11432; b) D. M. Guldi, G. M. A. Rahman, F. Zerbetto, M. Prato, *Acc. Chem. Res.* **2005**, *38*, 871; c) T. Hasobe, S. Fukuzumi, P. V. Kamat, *J. Phys. Chem. B* **2006**, *110*, 25477; d) H. Imahori, T. Umeyama, *J. Phys. Chem. C* **2009**, *113*, 9029; e) T. Hasobe, *Phys. Chem. Chem. Phys.* **2010**, *12*, 44.

[21] A. K. Burrell, D. L. Officer, P. G. Plieger, D. C. W. Reid, *Chem. Rev.* **2001**, *101*, 2751.

[22] a) F. Wessendorf, J. F. Gnichwitz, G. H. Sarova, K. Hager, U. Hartnagel, D. M. Guldi, A. Hirsch, *J. Am. Chem. Soc.* **2007**, *129*, 16057; b) G. R. Geier, B. J. Littler, J. S. Lindsey, *J. Chem. Soc. Perkin Trans.* **2001**, *2*, 712; c) J. S. Lindsey, S. Prathapan, T. E. Johnson, R. W. Wagner, *Tetrahedron* **1994**, *50*, 8941; d) J. S. Lindsey, R. W. Wagner, *J. Org. Chem.* **1989**, *54*, 828.

[23] S. Giordani, J. F. Colomer, F. Cattaruzza, J. Alfonsi, M. Meneghetti, M. Prato, D. Bonifazi, *Carbon* **2009**, *47*, 578.

[24] R. Marega, G. Accorsi, M. Meneghetti, A. Parisini, M. Prato, D. Bonifazi, *Carbon* **2009**, *47*, 675.

[25] J. Liu, A. G. Rinzler, H. Dai, J. H. Hafner, R. K. Bradley, P. J. Boul, A. Lu, T. Iverson, K. Shelimov, G. P. Huffman, F. Rodriguez-Marcias, Y. S. Shon, R. Lee, D. T. Colbert, R. E. Smalley, *Science* **1998**, *280*, 1253.

[26] a) W. Huang, Y. Lin, S. Taylor, J. Gaillard, A. M. Rao, Y. P. Sun, *Nano Lett.* **2002**, *2*, 231; b) R. Marega, V. Aroulmoji, M. Bergamin, L. Feruglio, F. Dinon, A. Bianco, E. Murano, M. Prato, *ACS Nano* **2010**, *4*, 2051.

[27] a) E. Xenogiannopoulou, M. Medved, K. Iliopoulos, S. Couris, M. G. Papadopoulos, D. Bonifazi, C. Sooambar, A. Mateo-Alonso, M. Prato, *ChemPhysChem* **2007**, *8*, 1056; b) N. Armaroli, G. Accorsi, F. Song, A. Palkar, L. Echegoyen, D. Bonifazi, F. Diederich, *Chem PhysChem* **2005**, *6*, 732; c) D. Bonifazi, H. Spillmann, A. Kiebele, M. de Wild, P. Seiler, F. Cheng, H.-J. Güntherodt, T. Jung, F. Diederich, *Angew. Chem. Int. Ed.* **2004**, *43*, 4759; d) N. Armaroli, G. Marconi, L. Echegoyen, J.-P. Bourgeois, F. Diederich, *Chem. Eur. J.* **2000**, *6*, 1629.

[28] J. Iehl, M. Vartanian, M. Holler, J.-F. Nierengarten, B. Delavaux-Nicot, J.-M. Strub, A. Van Dorsselaer, Y. Wu, J. Mohanraj, K. Yoosaf, N. Armaroli, *J. Mater. Chem.* **2011**, *21*, 1562.

[29] M. A. Fazio, A. Durandin, N. V. Tkachenko, M. Niemi, H. Lemmetyinen, D. I. Schuster, *Chem. Eur. J.* **2009**, *15*, 7698.

[30] N. Armaroli, *Fullerenes: From Synthesis to Optoelectronic Properties*, (Ed: D. M. Guldi), Kluwer Academic Publishers, Dordrecht **2002**.

[31] a) K. H. Le Ho, L. Rivier, B. Jousselme, P. Jegou, A. Filoramo, S. Campidelli, *Chem. Commun.* **2010**, *46*, 8731; b) C. Richard, F. Balavoine, P. Schultz, T. W. Ebbesen, C. Mioskowski, *Science* **2003**, *300*, 775.

[32] V. Sgobba, G. M. A. Rahman, D. M. Guldi, N. Jux, S. Campidelli, M. Prato, *Adv. Mater.* **2006**, *18*, 2264.

[33] This experiment is not possible in DMF due to insufficient dissolved oxygen content and low diffusion constant.

[34] J. Iehl, M. Vartanian, M. Holler, J.-F. Nierengarten, B. Delavaux-Nicot, J.-M. Strub, A. Van Dorsselaer, Y. Wu, J. Mohanraj, K. Yoosaf, N. Armaroli, *J. Mater. Chem.* **2010**, *21*, 1562.

[35] The transient decay measurement was not carried out on **1@DWCNTs** due to the poor loading of porphyrins. Also the transient absorption spectra were not taken for hybrid materials due to low loading of porphyrins.

[36] a) D. L. Akins, H.-R. Zhu, C. Guo, *J. Phys. Chem.* **1996**, *100*, 5420; b) Y. Arai, H. Segawa, *Chem. Commun.* **2010**, *46*, 4279; c) M. A. Castriciano, A. Romeo, V. Villari, N. Micali, L. M. Scolaro, *J. Phys. Chem. B* **2003**, *107*, 8765; d) A. Huijser, B. M. J. M. Suijkerbuijk, R. J. M. Klein Gebbink, T. J. Savenije, L. D. A. Siebbeles, *J. Am. Chem. Soc.* **2008**, *130*, 2485; e) X. Li, D. Li, W. Zeng, G. Zou, Z. Chen, *J. Phys. Chem. B* **2007**, *111*, 1502; f) G. E. O'Keefe, J. J. M. Halls, C. A. Walsh, G. J. Denton, R. H. Friend, H. L. Anderson, *Chem. Phys. Lett.* **1997**, *276*, 78; g) J. M. Ribo, J. Crusats, J.-A. Farrera, M. L. Valero, *Chem. Commun.* **1994**, *6*, 681.

[37] S. Verma, A. Ghosh, A. Das, H. N. Ghosh, *J. Phys. Chem. B* **2011**, *114*, 8327.

[38] M. Kasha, H. R. Rawls, M. A. El-Bayoumi, *Pure Appl. Chem.* **1965**, *11*, 371.

[39] π-π interactions between porphyrin and DWCNTs are insignificant due to high carboxylic acid functionalities on CNTs.

[40] a) H. Ago, K. Petritsch, M. S. P. Shaffer, A. H. Windle, R. H. Friend, *Adv. Mater.* **1999**, *11*, 1281; b) N. M. Dissanayake, Z. Zhong, *Nano Lett.* **2011**, *11*, 286; c) A. J. Miller, R. A. Hatton, S. R. P. Silva, *Appl. Phys. Lett.* **2006**, *89*, 133117; d) S. Mitra, C. Li, Y. H. Chen, Y. B. Wang, Z. Iqbal, M. Chhowalla, *J. Mater. Chem.* **2007**, *17*, 2406; e) M.-C. Wu, Y.-Y. Lin, S. Chen, H.-C. Liao, Y.-J. Wu, C.-W. Chen, Y.-F. Chen, W.-F. Su, *Chem. Phys. Lett.* **2009**, *468*, 64.

[41] a) E. Kymakis, G. A. J. Amaratunga, *Appl. Phys. Lett.* **2002**, *80*, 112; b) A. F. Nogueira, B. S. Lomba, M. A. Soto-Oviedo, C. R. D. Correia, P. Corio, C. A. Furtado, I. A. Hummelgen, *J. Phys. Chem. C* **2007**, *111*, 18431; c) B. Pradhan, S. K. Batabyal, A. J. Pal, *Appl. Phys. Lett.* **2006**, *88*, 093106.

[42] E. Klimov, W. Li, X. Yang, G. G. Hoffmann, J. Loos, *Macromolecules* **2006**, *39*, 4493.